Manganese-enhancedmagnetic resonance imaging in dilated cardiomyopathy and hypertrophic cardiomyopathy

ESC European Society of Cardiology

European Heart Journal - Cardiovascular Imaging (2020) **00**, 1–10
doi:10.1093/ehjci/jeaa273

Manganese-enhanced magnetic resonance imaging in dilated cardiomyopathy and hypertrophic cardiomyopathy

N.B. Spath[1,2,3,*†], T. Singh[1,2,3†], G. Papanastasiou [1,3], L. Kershaw [3,4], A.H. Baker[1], R.L. Janiczek[5], G.S. Gulsin[6], M.R. Dweck[1,2,3], G. McCann [6], D.E. Newby[1,2,3], and S.I. Semple[1,3]

[1]BHF/University Centre for Cardiovascular Science, University of Edinburgh, Edinburgh, EH16 4SA, UK; [2]Edinburgh Heart Centre, Royal Infirmary of Edinburgh, Edinburgh, EH16 4SB, UK; [3]Edinburgh Imaging, University of Edinburgh, Edinburgh, EH16 4TJ, UK; [4]Centre for Inflammation Research, University of Edinburgh, Edinburgh, EH16 4TJ, UK; [5]Department of Clinical Imaging, GlaxoSmithKline, Gunnels Wood Road, Stevenage, Hertfordshire, SG1 2NY, UK; and [6]Department of Cardiovascular Sciences, University of Leicester, NIHR Leicester Biomedical Research Centre, Glenfield Hospital, Leicester, LE3 9QP, UK

Received 1 July 2020; editorial decision 15 September 2020; accepted 17 September 2020

Aims The aim of this study is to quantify altered myocardial calcium handling in non-ischaemic cardiomyopathy using magnetic resonance imaging.

Methods and results Patients with dilated cardiomyopathy ($n = 10$) or hypertrophic cardiomyopathy ($n = 17$) underwent both gadolinium and manganese contrast-enhanced magnetic resonance imaging and were compared with healthy volunteers ($n = 20$). Differential manganese uptake (Ki) was assessed using a two-compartment Patlak model. Compared with healthy volunteers, reduction in T1 with manganese-enhanced magnetic resonance imaging was lower in patients with dilated cardiomyopathy [mean reduction 257 ± 45 (21%) vs. 288 ± 34 (26%) ms, $P < 0.001$], with higher T1 at 40 min (948 ± 57 vs. 834 ± 28 ms, $P < 0.0001$). In patients with hypertrophic cardiomyopathy, reductions in T1 were less than healthy volunteers [mean reduction 251 ± 86 (18%) and 277 ± 34 (23%) vs. 288 ± 34 (26%) ms, with and without fibrosis respectively, $P < 0.001$]. Myocardial manganese uptake was modelled, rate of uptake was reduced in both dilated and hypertrophic cardiomyopathy in comparison with healthy volunteers (mean Ki 19 ± 4, 19 ± 3, and 23 ± 4 mL/100 g/min, respectively; $P = 0.0068$). In patients with dilated cardiomyopathy, manganese uptake rate correlated with left ventricular ejection fraction ($r^2 = 0.61$, $P = 0.009$). Rate of myocardial manganese uptake demonstrated stepwise reductions across healthy myocardium, hypertrophic cardiomyopathy without fibrosis and hypertrophic cardiomyopathy with fibrosis providing absolute discrimination between the healthy myocardium and fibrosed myocardium (mean Ki 23 ± 4, 19 ± 3, and 13 ± 4 mL/100 g/min, respectively; $P < 0.0001$).

Conclusion The rate of manganese uptake in both dilated and hypertrophic cardiomyopathy provides a measure of altered myocardial calcium handling. This holds major promise for the detection and monitoring of dysfunctional myocardium, with the potential for early intervention and prognostication.

Keywords manganese-enhanced magnetic resonance imaging • MEMRI • non-ischaemic cardiomyopathy

*Corresponding author. Tel: +44 (0) 131 242 6427. E-mail: nick.spath@ed.ac.uk
†These authors contributed equally to this work.

Introduction

Cardiomyopathy represents a broad spectrum of clinical diseases which cause myocardial dysfunction leading to symptoms and signs of congestive cardiac failure. Whilst the aetiology is well characterized in ischaemic cardiomyopathy, non-ischaemic cardiomyopathies encompass a broad range of diseases that include genetic, acquired, and mixed aetiologies.[1] Advances in cardiac magnetic resonance imaging can help establish the aetiology of, and risk stratify patients with, dilated cardiomyopathy using techniques that include detection of fibrosis with late gadolinium enhancement and global longitudinal strain analysis.[2,3] However, there remains a relative lack of features discriminating the causes of some forms of non-ischaemic cardiomyopathy as well as the assessment of myocardial pathophysiology, disease severity, and disease progression.[2,4]

Hypertrophic cardiomyopathy represents another population of patients at-risk of heart failure, but with a distinct pathophysiology. These genetic disorders of sarcomeric proteins cause abnormal myocyte architecture and increased left ventricular wall thickness resulting in diastolic and systolic dysfunction.[5] Tissue characterization with cardiac magnetic resonance imaging has improved discrimination of hypertrophic cardiomyopathy phenocopies and defines macroscopic myocardial fibrosis with late gadolinium enhancement.[3,6,7] T1 mapping with extracellular volume quantification has also shown potential in adding to current risk stratification.[8,9] However, the techniques of late gadolinium enhancement and pre- and post-contrast T1 mapping do not provide information on cardiomyocyte function due to the extracellular distribution of gadolinium-based contrast media. This limits the ability to detect very early myocardial dysfunction and understand the *in vivo* pathophysiology of different disease states.

Manganese-enhanced magnetic resonance imaging has been well described in animal and human models showing the potential to assess myocardial calcium handling directly.[10–12] Here, manganese behaves as an analogue of calcium and is rapidly taken up by viable myocardium.[13,14] We have shown that manganese enhancement tracks with myocardial contractility and uptake is absent following acute myocardial infarction.[10] Furthermore, we have demonstrated that direct quantification of myocardial viability using manganese-enhanced magnetic resonance imaging is directly comparable with that of ^{18}F-fluorodeoxyglucose positron emission tomography.[12] However, despite these and other studies,[10,15–17] it has yet to be established whether manganese-enhanced magnetic resonance imaging can detect alterations in myocardial calcium handling and contractility in non-ischaemic cardiomyopathies. The objective of this proof-of-concept study was therefore to evaluate the ability of manganese-enhanced magnetic resonance imaging to detect altered myocardial calcium handling in patients with dilated or hypertrophic cardiomyopathy.

Methods

This was a single-centre open-label observational cohort study (NCT03607669, EudraCT number 2016-003782-25) which was carried out in accordance with the Declaration of Helsinki, the favourable ethical opinion of the South East Scotland Research Ethics Committee 2 (17/SS/0055) and with written informed consent from all participants.

Patients

Adult patients (≥18 years of age) with non-ischaemic dilated cardiomyopathy and hypertrophic cardiomyopathy were recruited from the Edinburgh Heart Centre between May 2018 and July 2019. Diagnosis of dilated cardiomyopathy and hypertrophic cardiomyopathy was based on echocardiography or magnetic resonance imaging according to European Society of Cardiology guidelines.[18]Non-ischaemic dilated cardiomyopathy was defined by the presence of impaired left ventricular systolic function (ejection fraction ≤50% within 12 months) and left ventricular dilatation (left ventricular end-diastolic volume >117% adjusted for age and body-surface area), in the absence of abnormal loading conditions (hypertension and valvular disease) and coronary artery disease.[18] Hypertrophic cardiomyopathy was defined as left ventricular hypertrophy (left ventricular wall thickness ≥15 mm in any segment) in the absence of haemodynamic stresses.[18] Presence of diastolic dysfunction in hypertrophic cardiomyopathy was based was defined on transthoracic echocardiography as per British Society of Transthoracic Echocardiography guidelines.[19]

All patients were required to have New York Heart Association Classes I–III heart failure, with stable symptoms and no change in maintenance therapy in the preceding month. Healthy volunteers were recruited as a control population and had no known pre-existing medical conditions. Exclusion criteria for all participants were any contraindication to magnetic resonance imaging, contraindications to manganese dipyridoxyl diphosphate administration (high degree atrioventricular block, history of torsades de pointes or prolonged QTc interval, obstructive liver disease, maintenance on calcium-channel blockade, or digoxin therapy), renal failure (estimated glomerular filtration rate <30 mL/min/1.73 m^2), New York Heart Association Class IV heart failure, and women of childbearing potential without a negative pregnancy test.

Magnetic resonance imaging

Magnetic resonance imaging was performed using a Siemens Magnetom Skyrafit 3 T scanner (Siemens Healthineers, Erlangen, Germany), with a dedicated 60-channel body array coil. All study participants underwent scanning with both late gadolinium enhancement and manganese-enhanced magnetic resonance imaging, ≥48 h apart and in random order. Images were acquired with ECG-gating and were breath-held in expiration. Cine imaging was acquired with retrospective ECG-gating, with standard steady-state free precession sequences (TrueFISP) in long and short-axis orientations as described previously.[10] T1 mapping was performed prospectively with shortened modified Look-Locker inversion recovery (WIP #1048 Siemens Healthineers). Quantitative estimation of T1 was performed in full short-axis stack from mitral valve annulus to apex and standard long-axis slices, with additional slices positioned appropriately to characterize pathology (repetition time = 388.8 ms; echo time = 1.07 ms; matrix = 256 × 115; slice thickness = 8 mm with 1.6 mm gap). T1 relaxation times were estimated before and after administration of gadolinium[20] and manganese-based contrast media.

Late gadolinium enhancement

Late-gadolinium enhancement images were acquired following intravenous administration of gadobutrol (0.1 mmol/kg; Gadovist, Bayer, Germany) using a single breath held phase-sensitive inversion recovery short-axis stack, and long axis orientations (repetition time = 820 ms; echo time = 1.04 ms; matrix = 192 × 81; slice thickness = 8 mm with 2 mm gap). A standardized inversion time of 400 ms was used and adjusted as required for optimal myocardial nulling. Post-contrast T1 mapping was performed prospectively with short-axis shortened modified Look-Locker inversion recovery stack 20 min post-contrast.

Serum haematocrit measured on the day of scanning was used to calculate extracellular volume.

Manganese-enhanced magnetic resonance imaging

Manganese-enhanced magnetic resonance imaging was achieved using intravenous infusion of manganese dipyridoxyl diphosphate [5 µmol/kg (0.1 mL/kg) at 1 mL/min; Exova SL Pharma, Wilmington, DE, USA]. T1 mapping was performed pre-contrast with full short-axis shortened modified Look-Locker inversion recovery stack as above (Supplementary data online, *Figure S1*). For patients, a single short-axis slice was identified by the supervising cardiologist, guided by the late gadolinium enhancement, native T1 maps and cine images to represent hypertrophied myocardium. For patients with hypertrophic cardiomyopathy, regions of maximal hypertrophy and fibrosis were selected and for dilated cardiomyopathy, a mid-ventricular short-axis slice was selected. A single short-axis T1 mapping was then performed at this slice location every 2.5 min for 40 min after starting contrast infusion, at which point a full short-axis shortened modified Look-Locker inversion recovery stack was repeated post-contrast (Supplementary data online, *Figure S1*). For healthy volunteers, a mid-ventricular slice was chosen for serial T1 mapping after manganese dipyridoxyl diphosphate infusion. Heart rate and blood pressure were measured for the duration of the scans.

Image analysis

All analysis of T1 maps, late-gadolinium enhancement and cine-derived volumetric and functional sequences was performed using Circle CVI (Circle Cardiovascular Imaging, CVI42 v5.3.6, Calgary, Canada) as described previously.[10] The operator was blinded to patients details and manganese-enhanced images were analysed separately from late-gadolinium images.

Kinetic modelling

Functional impairment by reduced calcium-channel activity was assessed on manganese-enhanced magnetic resonance imaging T1 maps. To quantify change in T1 over time, regions of interest were drawn in areas of pathological myocardium applied to all slices from 0 to 40 min. In patients with hypertrophic cardiomyopathy, regions of interest were drawn in regions of macroscopic fibrosis by late gadolinium enhancement as well as pathologically hypertrophied myocardium without clear fibrosis and non-hypertrophied non-fibrosed myocardium. For patients with dilated and diabetic cardiomyopathy, regions of interest were drawn in the mid-ventricular septal segments.

In brief, the model consists of (i) a reversible compartment (v_e), comparable to intravascular and interstitial space and (ii) an irreversible compartment (v_i) where irreversible accumulation of the contrast agent is anticipated, comparable to the intracellular space. The arterial concentration (derived from blood pool T1) represents contrast agent delivery into myocardial tissue and constitutes the arterial input function (Supplementary data online, *Figure S2*).

Skjöld *et al.*[21] have previously derived a Patlak model adaptation for cardiac manganese-enhanced magnetic resonance imaging, demonstrating an apparent unidirectional influx constant (*Ki*) for the transfer of manganese from plasma to irreversible compartments (v_i) can be measured using Eq. (1):

$$\frac{C_t(t)}{C_a(t)} = Ki\ \frac{\int_0^t C_a(\tau)d\tau}{C_a(t)} + v_e \tag{1}$$

where C_t and C_a are the manganese concentration in myocardial tissue and blood pool (arterial input function) respectively. This expression is equivalent to the Patlak formulation[22] and describes that if a contrast medium is irreversibly trapped in the tissue within the imaging time frame, the instantaneous tissue concentration divided by the instantaneous arterial concentration plotted against the integrated arterial concentration divided by the instantaneous arterial concentration, will result in linearization of the data. The gradient of this line represents the apparent unidirectional influx constant *Ki*, which in turn equals:

$$Ki = \frac{k1 \times k3}{k2 + k3} \tag{2}$$

where $k1$, $k2$, and $k3$ are the individual rate constants of the compartmental model presented (Supplementary data online, *Figure S2*). To derive the manganese concentrations C_t and C_a as a function of time to be used in Eq. (1), the following equation was used:

$$R_1(t) = R_1\ (0) + r_1 C(t) \tag{3}$$

where $R_1 = 1/T_1$, $R_1(0)$ is the native longitudinal relaxation rate and $R_1(t)$ is the longitudinal relaxation rate at time t of manganese contrast enhancement, r_1 is the relaxivity and $C(t)$ is the concentration of the contrast agent at time t. Using Eq. (3), C_t and C_a were calculated for each successive T_1 map derived in the tissue and blood pool before, during and after contrast infusion for the 40 min period of the manganese-enhanced magnetic resonance imaging protocol (Supplementary data online, *Figure S1*). The Patlak model employed here has previously been shown as an effective method of estimating intracellular influx of manganese in the context of imaging with MnDPDP in the same dose and formulation used in the present study.[21,22]

Contrast kinetics modelling was performed using in-house software[20] developed in Matlab (Version R2016a, MathWorks Inc., Natick, MA, USA) based on a two-compartment model identical to that previously applied to cardiac manganese-enhanced magnetic resonance imaging with manganese dipyridoxyl diphosphate.[21]

Statistical analysis

All statistical analysis was performed with GraphPad Prism (GraphPad Software v8.0.2, San Diego, CA, USA). Continuous data were assessed for normality using the D'Agostino-Pearson test. Categorical baseline variables were compared using Fisher's exact test. Values are mean ± standard deviation unless otherwise stated. To compare cardiac function and change in myocardial manganese uptake in patients and healthy volunteers, volumetric assessment, and parametric mapping values were compared using paired or unpaired *t*-tests, Wilcoxon or Mann–Whitney tests, and analysis of variance and co-variance or Kruskal–Wallis tests as appropriate. Statistical significance was taken as two-sided $P < 0.05$.

Results

Ten patients with non-ischaemic dilated cardiomyopathy and 20 patients with hypertrophic cardiomyopathy were recruited. Three patients in the hypertrophic cardiomyopathy cohort withdrew (two had claustrophobia and one developed high degree atrioventricular block prior to infusion), leaving 17 who completed the study protocol. A cohort of 20 healthy volunteers was used as a contemporaneous control group (*Table 1*).[23] All patients completed late gadolinium-enhanced and manganese-enhanced magnetic resonance imaging scans, at least 48 h apart.

Most patients had idiopathic non-ischaemic dilated cardiomyopathy, with three with history of familial dilated cardiomyopathy. Over half of patients with hypertrophic cardiomyopathy had genetic testing with seven gene positive cases. The patient groups were older than healthy volunteers but were well matched for gender and body mass index (*Table 1*). Patients had higher left ventricular mass index and

Table 1 Baseline clinical characteristics of study participants

	Healthy volunteers ($n = 20$)	Patients with non-ischaemic cardiomyopathy ($n = 27$)	
		Dilated cardiomyopathy ($n = 10$)	Hypertrophic cardiomyopathy ($n = 17$)
Male	13 (65)	6 (60)	10 (59)
Age (years)	42 ± 11	57 ± 10	65 ± 7
Body-mass index (kg/m^2)	26.0 ± 2.9	28.1 ± 3.1	29.1 ± 5.4
Aetiology			
Idiopathic	—	6 (60)	—
Genetic	—	3 (30)	17(100)
Drug induced	—	1 (10)	—
Genetic testing			
Positive	—	3 (30)	7 (41)
Negative	—	1 (10)	4 (24)
Not done	—	6 (60)	6 (35)
Echocardiographic Findings			
LV systolic dysfunction	0 (0)	10 (100)	0 (0)
LV diastolic dysfunction	0 (0)	—	17 (100)
Past medical history	—		
Hypertension	0	1 (10)	2 (12)
Ischaemic heart disease	0	2 (20)	1 (6)
Hypercholesterolaemia	0	2 (20)	0
Atrial fibrillation/flutter	0	1 (10)	2 (12)
Cerebrovascular disease	0	1 (10)	0
Diabetes mellitus	0	1 (10)	0
Medications			
Antiplatelet therapy	0	5 (50)	2 (12)
β-Blocker therapy	0	10 (100)	8 (47)
ACE inhibitor/ARB therapy	0	6 (60)	6 (35)
MRA therapy	0	10 (100)	0
Statin therapy	0	5 (50)	2 (12)
Anticoagulation therapy	0	0	0
Smoking status			
Non-smoker	18	6 (60)	13 (76)
Ex-smoker	2	3 (30)	4 (24)
Current smoker	0	1 (10)	0

n (%) or mean ± standard deviation.
LV, left ventricular; ACE, angiotensin-converting enzyme; ARB, angiotensin receptor blocker; MRA, mineralocorticoid receptor antagonist.

extracellular volume fraction ($P = 0.0002$ and $P < 0.0001$ respectively, *Table 2*).

Administration of manganese dipyridoxyl diphosphate was well tolerated by all participants, with a mean infusion time of 8 min. No adverse events or side-effects were recorded by 7 days of follow-up in any participant. There were no changes in ECG variables, heart rate, or blood pressure during infusion of manganese dipyridoxyl diphosphate (Supplementary data online, *Figure S3*, all $P > 0.1$).

Patients with non-ischaemic dilated cardiomyopathy

In comparison with healthy volunteers, patients with dilated cardiomyopathy had lower ejection fraction and higher cardiac volumes (*Table 2*). Native myocardial T1 was higher in patients with non-ischaemic dilated cardiomyopathy (1204 ± 70 vs. 1123 ± 36 ms; *Figure 1*). During manganese dipyridoxyl diphosphate infusion, myocardial T1 values demonstrated a rapid initial descent followed by a gradual and sustained reduction that was similar to the myocardium of healthy volunteers. However, mean reductions in T1 values were less marked in patients with dilated cardiomyopathy [mean reduction 257 ± 45 (21%) vs. 288 ± 34 (26%) ms, ANCOVA $P = 0.03$], resulting in higher T1 values at 40 min (948 ± 57 vs. 834 ± 28 ms, ANCOVA $P = 0.0011$; *Figure 2*).

Kinetic modelling demonstrated a lower rate of myocardial manganese uptake in patients with dilated cardiomyopathy compared with healthy volunteers (mean *Ki* 19 ± 4 and 23 ± 4 mL/100 g/min,

Table 2 Baseline magnetic resonance imaging characteristics of study participants

	Healthy control ($n = 20$)	Non-ischaemic cardiomyopathy ($n = 27$)		ANOVA *P*-value	*P*-Value (DCM vs. HCM)
		DCM ($n = 10$)	HCM ($n = 17$)		
LVEDVI (mL/m^2)	74.7 ± 14.4	111.4 ± 39.4	62.9 ± 10.1	<0.0001	0.00052
LVESVI (mL/m^2)	26.8 ± 7.3	74.0 ± 39.2	15.2 ± 4.4	<0.0001	0.00002
Stroke volume index (mL/m^2)	47.9 ± 9.1	37.3 ± 8.3	47.7 ± 7.2	0.0011	0.002
Ejection fraction (%)	64.4 ± 5.5	34.7 ± 13.6	76.2 ± 4.8	<0.0001	<0.0001
LV mass index (g/m^2)	57.9 ± 13.1	76.8 ± 20.7	86.7 ± 27.1	0.0002	0.329
Extracellular volume (%)	27.1 ± 3.6	33.8 ± 2.7	31.3 ± 2.5	<0.0001	0.022
Native T1-septum (ms)	1123 ± 36	1206 ± 57	1183 ± 42	<0.0001	0.239
MEMRI T1-septum (ms)	835 ± 28	927 ± 43	899 ± 34	<0.0001	0.073
Native T1-fibrosis (ms)	—	—	1392 ± 215		
MEMRI T1-fibrosis (ms)	—	—	1141 ± 209		
Late gadolinium enhancement (% LV)	—	—	13 ± 4		
Influx constant (*Ki*/mL/100 g/min)					
Myocardial septum	23 ± 4	19 ± 4.0	19 ± 3	<0.0001	0.941
Fibrosis	—	—	13 ± 4		

Mean ± standard deviation or median ± interquartile range.
HCM, hypertrophic cardiomyopathy; DCM, non-ischaemic cardiomyopathy, LVEDVI, indexed left ventricular end-diastolic volume; LVESVI, indexed left ventricular end-systolic volume; MEMRI, manganese-enhanced magnetic resonance imaging; LV, left ventricular; ANOVA, analysis of variance.

respectively, $P = 0.0068$; *Figure 3*). The rate of myocardial manganese uptake (by influx constant) correlated with left ventricular ejection fraction in patients with dilated cardiomyopathy ($r^2 = 0.61$, $P = 0.009$, *Figure 4*).

Patients with hypertrophic cardiomyopathy

In comparison with healthy volunteers, patients with hypertrophic cardiomyopathy had higher ejection fraction, lower cardiac volumes and diastolic dysfunction to varying degrees (*Tables 1 and 2*). Native T1 values of the myocardium were higher in patients with hypertrophic cardiomyopathy compared with healthy volunteers (1183 ± 42 vs. 1123 ± 36 ms; *Figure 1*). In patients, there were discrete foci of bright late gadolinium enhancement indicating dense fibrosis which showed markedly different T1 profiles following manganese dipyridoxyl diphosphate infusion, with T1 recovering towards baseline values similar to the blood pool (*Figure 5*). In areas of hypertrophied myocardium without discrete late gadolinium enhancement, T1 values following manganese dipyridoxyl diphosphate infusion demonstrated a gradual but continued reduction in T1 values over the 40-min period. Manganese-enhanced T1 values were higher in regions with and without discrete late gadolinium enhancement (908 ± 47 and 1140 ± 208 vs. 834 ± 28 ms in myocardium of healthy volunteers, both ANCOVA $P < 0.0001$). Mean reductions in T1 were lower in patients with and without fibrosis compared with healthy volunteers [mean reduction 252 ± 86 (18%) and 277 ± 34 (23%) vs. 288 ± 34 (26%) ms respectively, ANCOVA $P < 0.001$].

Kinetic modelling of myocardial manganese influx demonstrated stepwise reductions across healthy myocardium, hypertrophic cardiomyopathy without fibrosis and hypertrophic cardiomyopathy with fibrosis, providing clear demarcation between the healthy myocardium and fibrosed myocardium (mean *Ki* 23 ± 4, 19 ± 3 and 13 ± 4 mL/100 g/min; ANCOVA $P < 0.0001$; *Figure 3*).

Discussion

This is the first description of manganese-enhanced magnetic resonance imaging T1 mapping to detect abnormal myocardial cellular physiology in patients with non-ischaemic dilated cardiomyopathy or hypertrophic cardiomyopathy. Our findings suggest that alterations in myocardial calcium handling in cardiomyopathies can be detected and are associated with left ventricular systolic dysfunction as well as regions of fibrosis and scar formation. This novel approach has major potential for the detection, investigation, and management of patients with a range of cardiomyopathies.

Myocardial contraction is dependent on excitation-contraction coupling for which calcium homeostasis is essential. Dysfunctional calcium handling is a central feature of left ventricular dysfunction in patients with dilated cardiomyopathy, with alterations in calcium handling proteins[24] leading to reduced myocardial contractile function.[25,26] We have shown that manganese-enhanced magnetic resonance imaging detects clear abnormalities in myocardial calcium handling of patients with non-ischaemic dilated cardiomyopathy. Moreover, kinetic modelling demonstrated a direct correlation between myocardial manganese uptake and left ventricular ejection fraction. As such, this study confirms the presence of dysfunctional calcium handling in the myocardium of patients with non-ischaemic dilated cardiomyopathy. Furthermore, it provides a non-invasive imaging technique that has the potential to be used as a marker for risk stratification, disease progression, and response to therapy.[5]

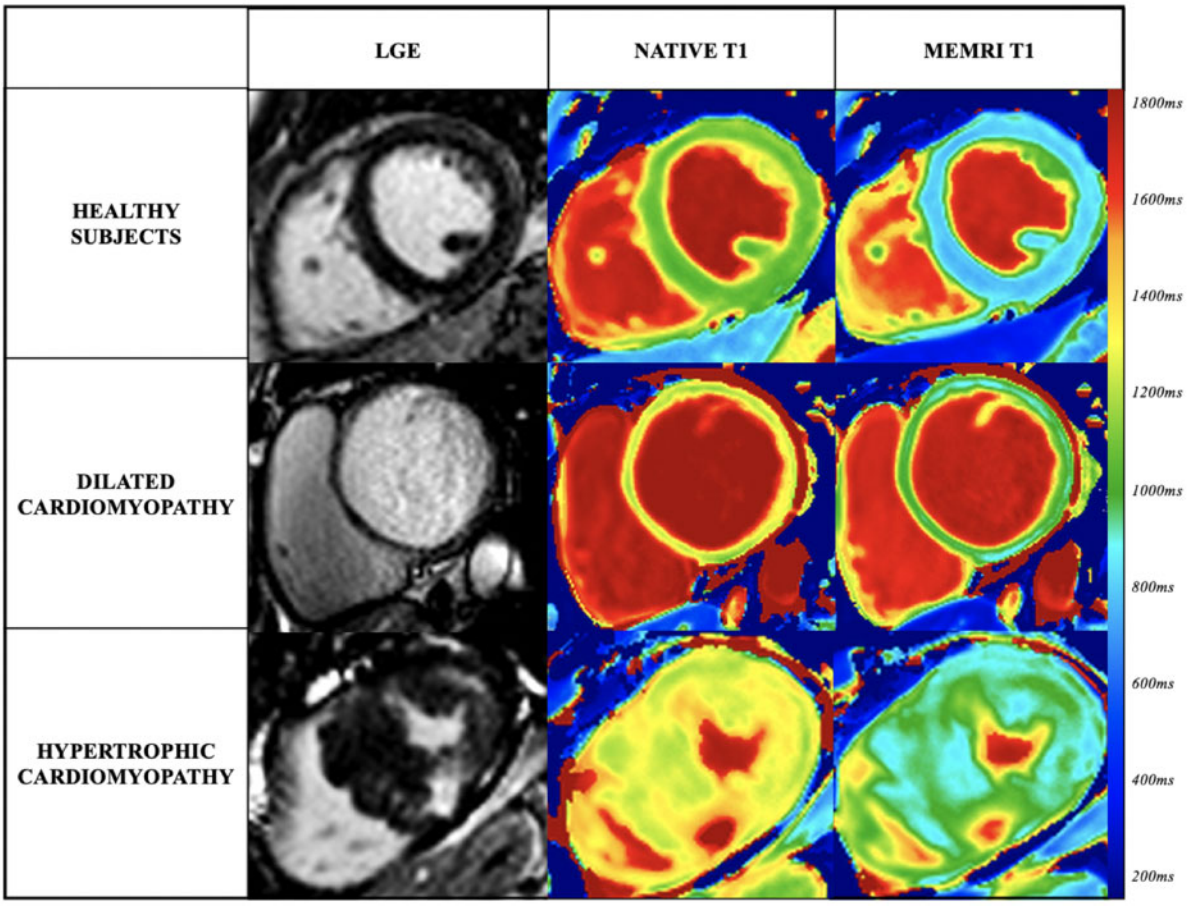

Figure 1 Late gadolinium enhanced, native T1 and manganese-enhanced magnetic resonance imaging in healthy volunteers and patients with non-ischaemic cardiomyopathy. Representative late gadolinium enhancement, native and manganese-enhanced magnetic resonance imaging T1 mapping in (*A*) healthy volunteer, (*B*) patient with dilated cardiomyopathy, and (*C*) patient with hypertrophic cardiomyopathy following manganese dipyridoxyl diphosphate infusion.

Detection of myocardial fibrosis with late gadolinium enhancement and global measures of cardiac performance, such as left ventricular ejection fraction, can help in monitoring disease and prognostication.[27] However, subtle myocyte dysfunction is difficult to detect and could be beneficial in highlighting patients who are at risk of deteriorating left ventricular function: a feature which is associated with poor cardiac outcomes.[28] In the present study, manganese-enhanced magnetic resonance imaging detected altered manganese uptake reflecting abnormal calcium handling in patients with severe phenotypes of non-ischaemic cardiomyopathy. Manganese-enhanced magnetic resonance imaging therefore has potential to go beyond myocardial fibrosis imaging and identify subclinical changes in calcium handling, a feature that could also be utilized in the early detection of patients who are at risk of heart failure prior to developing symptoms or signs of overt left ventricular dysfunction. This needs to be confirmed in future studies across a range of clinical phenotypes of cardiac disease.

In patients with hypertrophic cardiomyopathy, the left ventricular ejection fraction was preserved or supranormal with diastolic dysfunction seen in all cases. Despite this, myocardial manganese-enhanced magnetic resonance imaging T1 and native T1 were higher in regions of hypertrophy without discrete late gadolinium enhancement. The rate of manganese influx into pathologically hypertrophied myocardium was reduced. This indicates the presence of abnormal myocardial calcium handling in hypertrophied myocardium with predominantly diastolic impairment. Diastolic dysfunction in hypertrophic cardiomyopathy is multifactorial, and includes prolonged and disordered ventricular relaxation, decreased chamber compliance, and abnormal calcium cycling.[29] Increases in calcium entry through L-type calcium channels combined with reduced calcium extrusion and lower sarcoplasmic reticulum calcium adenosine triphosphotase expression result in elevated intracellular calcium concentration. Furthermore, dysfunctional calcium handling appears to precede alterations in metabolic activity[30] and is associated with an increased risk of arhythmogenesis.[31] As such, manganese-enhanced magnetic resonance could be used to detect the earlier signs of altered calcium handling, a surrogate marker of disease progression and prognostication.[32]

In patients with hypertrophic cardiomyopathy, the recovery of myocardial T1 values within dense regions of severe fibrosis was

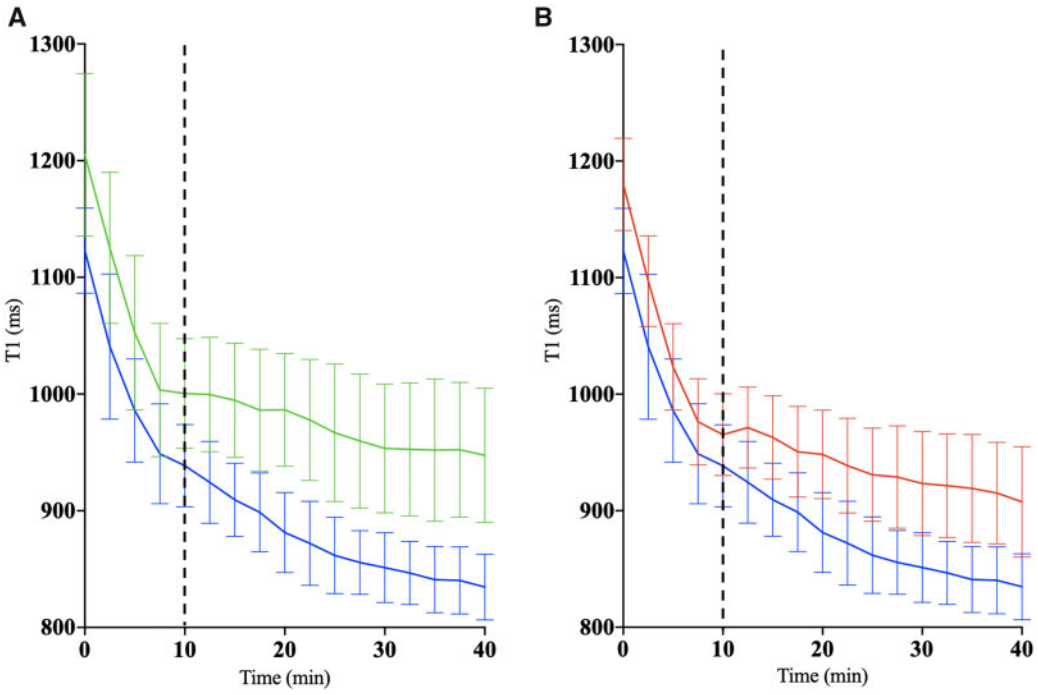

Figure 2 Native and manganese-enhanced magnetic resonance imaging T1 profiles in patients with non-ischaemic cardiomyopathy. Representative mean T1 profiles of myocardial regions of interest over time following manganese dipyridoxyl diphosphate in (*A*) patient with dilated cardiomyopathy (green, *n* = 10), compared with healthy volunteers (blue, *n* = 20) and (*B*) patient with hypertrophic cardiomyopathy (red, *n* = 17), compared with healthy volunteers (blue, *n* = 20). Manganese dipyridoxyl diphosphate was infused from time 0 to 10 min (dashed line). Error bars are standard deviation of the mean.

similar to that observed in the blood pool. We have previously described a similar profile of recovery in regions of transmural acute myocardial infarction.[10] This is consistent with the marked reduction in manganese uptake due to the presence of non-viable myocardium and non-functional fibrotic tissue scar. This ability to differentiate and track viable myocardium could play a role in the assessment of reversible causes of cardiomyopathies which show transient myocardial dysfunction.

After administration, biotransformation of manganese dipyridoxyl diphosphate occurs by dephosphorylation and transmetallation with zinc, enabling intracellular manganese uptake as demonstrated in vitro where tissue uptake and renal clearance occur rapidly.[33,34]Manganese-based contrast media have previously been reported to cause acute myocardial suppressant effects. In preclinical studies, unchelated manganese chloride produced very high free manganese ion concentrations causing negative inotropy and cardiovascular instability.[35] We used a custom manufactured dipyridoxyl diphosphate chelation of manganese which markedly reduces free unbound manganese ions. This formulation of manganese was previously approved for clinical use (Teslascan®)[36] but was withdrawn from the US market in 2003[37] and the EU market in 2010[38] because it was not commercially viable. In Phase 3 clinical trials,[39] mild to moderate side effects were reported in 1–7% of participants and included headache and flushing. In the present study, we observed no adverse events or side effects despite including patients with marked left ventricular dysfunction and ejection fractions of <25%. Furthermore, there were no instances of haemodynamic compromise or cardiac arrhythmia during, or up to 30 min following, manganese administration, and no adverse symptoms or side effects reported at 7-day follow-up. This suggests that this formulation of manganese is safe even in those with left ventricular systolic dysfunction.

What are the clinical implications of our findings? In this study, we have undertaken manganese-enhanced magnetic resonance imaging T1 mapping in two populations of non-ischaemic cardiomyopathies and have demonstrated its ability to detect and to quantify altered myocardial calcium handling over and above existing methods of identifying myocardial fibrosis. This is not specific to non-ischaemic cardiomyopathies and could potentially be used to assess a wider range of cardiomyopathy phenotypes, although this has yet to be established. As expected, manganese-enhanced magnetic resonance imaging correlated with a range of left ventricular ejection fraction suggesting it has potential to track and to quantify more subtle gradations of myocardial dysfunction. Late-gadolinium enhancement and extracellular volume fraction imaging relies on abnormal tissue structure to identify regions of pathological myocardium. The ability of manganese-enhanced magnetic resonance imaging to detect altered calcium handling over time and quantify cellular myocardial function directly may transform our ability to assess myocardial function directly, enabling early detection, prognostication and assessment of

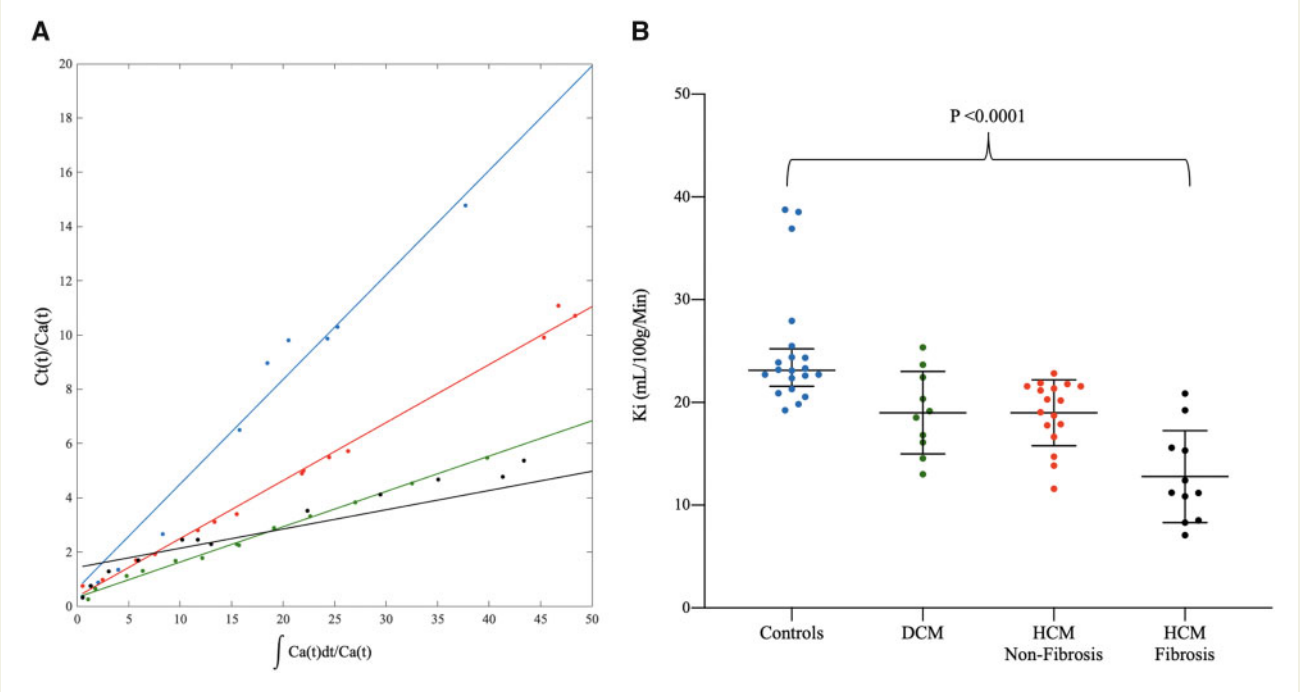

Figure 3 Differential manganese uptake in patients with non-ischaemic cardiomyopathy. Patlak plot (*A*) and kinetic modelling of manganese uptake (*B*) (*Ki*, influx constant) in patients with non-ischaemic cardiomyopathy. Each line represents a single representative individual. Healthy volunteers (blue), patients with dilated cardiomyopathy (green), patients with hypertrophic cardiomyopathy without fibrosis (red), and patients with hypertrophic cardiomyopathy with fibrosis (black).

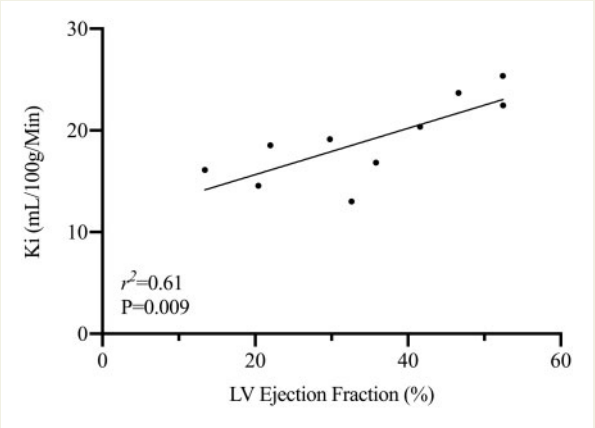

Figure 4 Manganese uptake vs. left ventricular ejection fraction in patients with dilated cardiomyopathy. Myocardial manganese uptake (by influx constant) in patients with dilated cardiomyopathy.

treatment efficacy. With optimization, this technique has potential to allow individualization of heart failure treatment, targeting optimal therapy to those most likely to benefit. Furthermore, early detection of altered calcium-handling in established or at-risk cardiomyopathy may enable earlier initiation of preventative therapy than previously possible, with the potential to improve long-term clinical outcomes. We therefore suggest that further investigation of reversible cardiomyopathies, such as stress cardiomyopathy and myocarditis, is a crucial next step to further our understanding of calcium dysfunction seen in the acute and chronic setting.

Our study has several limitations that should be considered. First, there have been prior concerns regarding toxicity as well as current lack of a marketed formulation of manganese. The chelated form used here retains the necessary properties for intracellular myocardial imaging whilst cardiac function remains uncompromised as demonstrated by the absence of haemodynamic or arrhythmic effects in published safety data.[40,41] Furthermore, we anticipate that the availability of such agents will increase following continued demonstration of its clinical and research utility. Secondly, calcium channel antagonists and digoxin reduce uptake of manganese dipyridoxyl diphosphate and as a result these medications were excluded. However, patients were maintained on other cardiac medications including β-blocker, angiotensin converting enzyme inhibitor, mineralocorticoid receptor antagonist, statin, and anti-platelet therapies. We cannot exclude an effect of these medications on our findings but in our previous work in patients with acute myocardial infarction, concomitant use of these medications did not influence manganese uptake in the myocardium remote from the site of infarction.[23] Thirdly, as a proof-of-concept study, the sample size is small, reflecting absence of prior data in this area on which to base accurate power calculations as the variance was unknown. Data from this study will facilitate ongoing and future studies to confirm the translational potential of this approach. Finally, we cannot rule out that calcium handling deteriorates with age and the fact that control subjects were younger than those

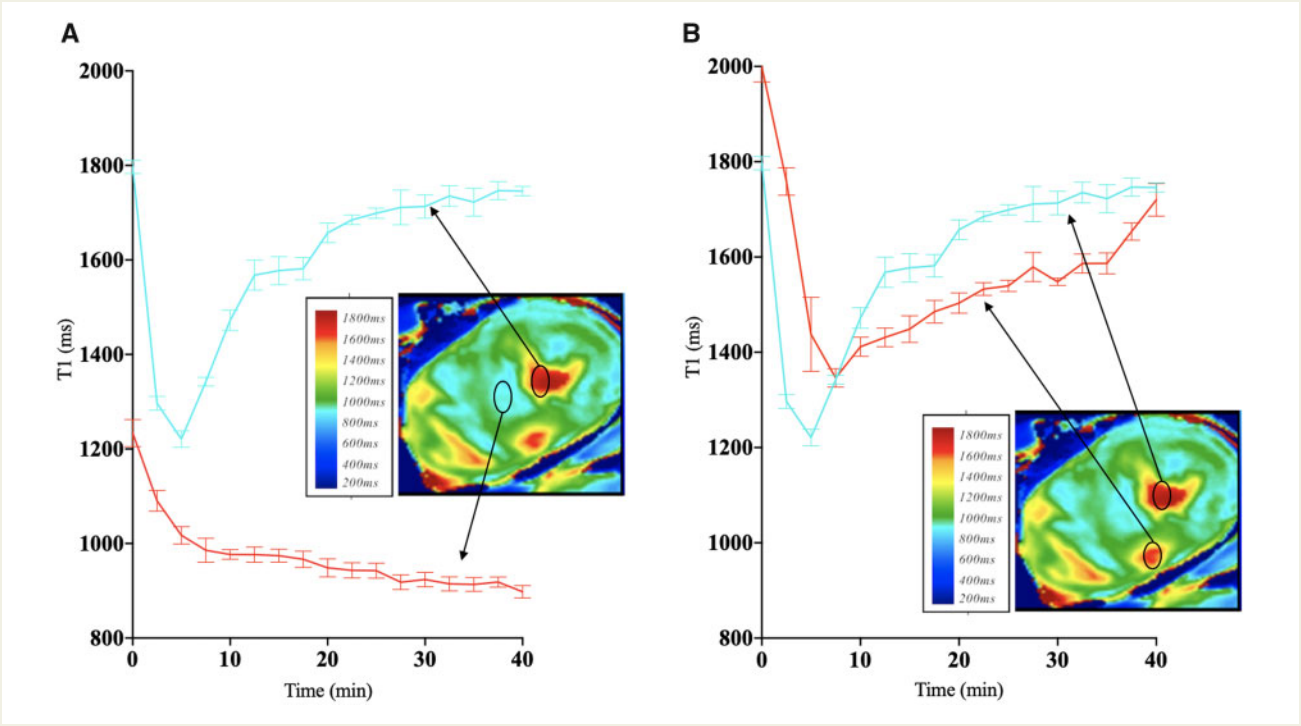

Figure 5 Manganese-enhanced magnetic resonance imaging in patients with hypertrophic cardiomyopathy. Representative manganese-enhanced magnetic resonance imaging T1 mapping image and T1 profile in a patient with hypertrophic cardiomyopathy in (*A*) hypertrophied myocardium without fibrosis (red), compared with blood pool (light blue) and (*B*) in hypertrophied myocardium with fibrosis (red), compared with blood pool (light blue). Manganese dipyridoxyl diphosphate was infused from time 0 to 10 min (dashed line). Error bars are standard deviation of the mean.

with cardiomyopathy could explain some of the observed reductions in manganese uptake. However, we found no correlation between age and manganese uptake in the healthy volunteers or our individual patient cohorts (data not shown).

Conclusion

We have described the first proof-of-concept T1 mapping study of manganese-enhanced magnetic resonance imaging in patients with non-ischaemic cardiomyopathy. Using kinetic modelling, we have shown that manganese-enhanced magnetic resonance imaging can detect dysfunctional myocardial calcium handling and can directly distinguish normal from pathological myocardium. We believe that manganese-enhanced magnetic resonance imaging holds major promise for the detection and monitoring of disease progression in non-ischaemic cardiomyopathy, with the potential for early intervention, tracking of response to therapy, and overall prognostication. Finally, its application to other areas of disease, such as reversible cardiomyopathies or detection of sub-clinical cardiomyopathies, warrants further investigation.

Supplementary data

Supplementary data are available at *European Heart Journal - Cardiovascular Imaging* online.

Acknowledgements

Grateful acknowledgements are made to Siemens Healthineers for provision of the WIP used in this study and the Edinburgh Imaging Facility radiographers.

Data availability

The data underlying this article may be shared on reasonable request to the corresponding author.

Funding

This work and N.B.S., T.S., A.H.B., G.S.G., M.R.D., and D.E.N. were supported by the British Heart Foundation (FS/17/19/32641, FS/14/78/31020, CH/09/002, RG/16/10/32375, and RE/18/5/34216). T.S. was supported by MRC (MR/T029153/1). GM was supported by a NIHR research professorship (RP-2017-08-ST2-007). D.E.N. was the recipient of a Wellcome Trust Senior Investigator Award (WT103782AIA). The Edinburgh Clinical Research Facilities and Edinburgh Imaging facility was supported by the National Health Service Research Scotland (NRS) through National Health Service Lothian Health Board.

Conflict of interest: D.E.N. and S.I.S. hold unrestricted educational grants from Siemens Healthineers.

References

1. Wu AH. Management of patients with non-ischaemic cardiomyopathy. *Heart* 2007;**93**:403–8.
2. Japp AG, Gulati A, Cook SA, Cowie MR, Prasad SK. The diagnosis and evaluation of dilated cardiomyopathy. *J Am Coll Cardiol* 2016;**67**:2996–3010.

3. Halliday BP, Gulati A, Ali A, Guha K, Newsome S, Arzanauskaite M *et al.* Association between midwall late gadolinium enhancement and sudden cardiac death in patients with dilated cardiomyopathy and mild and moderate left ventricular systolic dysfunction. *Circulation* 2017;**135**:2106–15.
4. Assomull RG, Shakespeare C, Kalra PR, Lloyd G, Gulati A, Strange J *et al.* Role of cardiovascular magnetic resonance as a gatekeeper to invasive coronary angiography in patients presenting with heart failure of unknown etiology. *Circulation* 2011;**124**:1351–60.
5. Reza N, Musunuru K, Owens AT. From hypertrophy to heart failure: what is new in genetic cardiomyopathies. *Curr Heart Fail Rep* 2019;**16**:157–67.
6. Dass S, Suttie JJ, Piechnik SK, Ferreira VM, Holloway CJ, Banerjee R *et al.* Myocardial tissue characterization using magnetic resonance noncontrast T1 mapping in hypertrophic and dilated cardiomyopathy. *Circ Cardiovasc Imaging* 2012;**5**:726–33.
7. Swoboda PP, McDiarmid AK, Page SP, Greenwood JP, Plein S. Role of T1 mapping in inherited cardiomyopathies. *Eur Cardiol Rev* 2016;**11**:96–101.
8. Hinojar R, Varma N, Child N, Goodman B, Jabbour A, Yu CY *et al.* T1 mapping in discrimination of hypertrophic phenotypes: hypertensive heart disease and hypertrophic cardiomyopathy: findings from the international T1 multicenter cardiovascular magnetic resonance study. *Circ Cardiovasc Imaging* 2015;**8**:e003285.
9. Swoboda PP, McDiarmid AK, Erhayiem B, Broadbent DA, Dobson LE, Garg P *et al.* Assessing myocardial extracellular volume by T1 mapping to distinguish hypertrophic cardiomyopathy from athlete's heart. *J Am Coll Cardiol* 2016;**67**:2189–90.
10. Spath NB, Lilburn DML, Gray GA, Page LM, Le Papanastasiou G, Lennen RJ *et al.* Manganese-enhanced T1 mapping in the myocardium of normal and infarcted hearts. *Contrast Media Mol Imaging* 2018;**2018**:1–13.
11. Skjöld A, Amundsen BH, Wiseth R, Støylen A, Haraldseth O, Larsson HBW *et al.* Manganese dipyridoxyl-diphosphate (MnDPDP) as a viability marker in patients with myocardial infarction. *J Magn Reson Imaging* 2007;**26**:720–7.
12. Spath N, Tavares A, Gray GA, Baker AH, Lennen RJ, Alcaide-Corral CJ *et al.* Manganese-enhanced T1 mapping to quantify myocardial viability: validation with 18F-fluorodeoxyglucose positron emission tomography. *Sci Rep* 2020;**10**(1):2018.
13. Toft KG, Hustvedt SO, Grant D, Martinsen I, Gordon PB, Friisk GA *et al.* Metabolism and pharmacokinetics of MnDPDP in man. *Acta Radiol* 1997;**38**:677–89.
14. Wang C, Gordon PB, Hustvedt SO, Grant D, Tufte Sterud A, Martinsen I *et al.* MR imaging properties and pharmacokinetics of MnDPDP in healthy volunteers. *Acta Radiol* 1997;**38**:665–76.
15. Du C, MacGowan GA, Farkas DL, Koretsky AP. Calibration of the calcium dissociation constant of Rhod2 in the perfused mouse heart using manganese quenching. *Cell Calcium* 2001;**29**:217–27.
16. Massaad CA, Pautler RG. Manganese-enhanced magnetic resonance imaging (MEMRI). *Methods Mol Biol* 2011;**711**:145–74.
17. Spath N, Tavares A, Gray GA, Baker AH, Lennen RJ, Alcaide-Corral CJ *et al.* Manganese-enhanced T1 mapping to quantify myocardial viability: validation with 18F-fluorodeoxyglucose positron emission tomography. *Sci Rep* 2020;**10**:2018.
18. Elliott P, Andersson B, Arbustini E, Bilinska Z, Cecchi F, Charron P *et al.* Classification of the cardiomyopathies: a position statement from the European Society of Cardiology working group on myocardial and pericardial diseases. *Eur Heart J* 2007;**29**:270–6.
19. Nagueh SF, Smiseth OA, Appleton CP, Byrd BF, Dokainish H, Edvardsen T *et al.* Recommendations for the evaluation of left ventricular diastolic function by echocardiography: an update from the American Society of Echocardiography and the European Association of Cardiovascular Imaging. *Eur Heart J Cardiovasc Imaging* 2016;**29**:277–314.
20. Papanastasiou G, Williams MC, Kershaw LE, Dweck MR, Alam S, Mirsadraee S *et al.* Measurement of myocardial blood flow by cardiovascular magnetic resonance perfusion: comparison of distributed parameter and Fermi models with single and dual bolus. *J Cardiovasc Magn Reson* 2015;**17**:17.
21. Skjöld A, Kristoffersen A, Vangberg TR, Haraldseth O, Jynge P, Larsson HBW. An apparent unidirectional influx constant for manganese as a measure of myocardial calcium channel activity. *J Magn Reson Imaging* 2006;**24**:1047–55.
22. Logan J. Graphical analysis of PET data applied to reversible and irreversible tracers. *Nucl Med Biol* 2000;**27**:661–70.
23. Spath N, Papanastasiou G, Singh T, Baker A, Janiczek R, McCann G *et al.* Manganese-enhanced T1 mapping for the detection of viable and stunned myocardium following myocardial infarction. *J Am Coll Cardiol* 2020;75(11 Supplement 1):1567.
24. Meyer M, Schillinger W, Pieske B, Holubarsch C, Heilmann C, Posival H *et al.* Alterations of sarcoplasmic reticulum proteins in failing human dilated cardiomyopathy. *Circulation* 1995;**92**:778–84.
25. Hasenfuss G, Pieske B. Calcium cycling in congestive heart failure. *J Mol Cell Cardiol* 2002;**113**:690–708.
26. Ren J, Gintant GA, Miller RE, Davidoff AJ. High extracellular glucose impairs cardiac E-C coupling in a glycosylation-dependent manner. *Am J Physiol - Hear Circ Physiol* 1997;**273**:H2876–H2883.
27. Kwong RY, Ge Y, Steel K, Bingham S, Abdullah S, Fujikura K *et al.* Cardiac magnetic resonance stress perfusion imaging for evaluation of patients with chest pain. *J Am Coll Cardiol* 2019;**74**:1741–55.
28. Nabeta T, Inomata T, Ishii S, Yazaki M, Fujita T, Iida Y *et al.* Dilated cardiomyopathy with re-worsening left ventricular ejection fraction. *Heart Vessels* 2019;**34**:95–103.
29. Geske JB, Ommen SR, Gersh BJ. Hypertrophic cardiomyopathy: clinical update. *JACC Hear Fail* 2018;**6**:364–75.
30. Kenny HC, Abel ED. Heart failure in type 2 diabetes mellitus. *Circ Res* 2019;**124**:121–41.
31. Coppini R, Ferrantini C, Mugelli A, Poggesi C, Cerbai E. Altered Ca2+ and Na+ homeostasis in human hypertrophic cardiomyopathy: implications for arrhythmogenesis. *Front Physiol* 2018;**9**:1391.
32. Viola HM, Hool LC. Impaired calcium handling and mitochondrial metabolic dysfunction as early markers of hypertrophic cardiomyopathy. *Arch Biochem Biophys* 2019;**655**:166–74.
33. Toft KG, Kindberg GM, Skotland T. Mangafodipir trisodium injection, a new contrast medium for magnetic resonance imaging: in vitro metabolism and protein binding studies of the active component MnDPDP in human blood. *J Pharm Biomed Anal* 1997;**15**:983–8.
34. Spath NB, Thompson G, Baker AH, Dweck MR, Newby DE, Semple SIK. Manganese-enhanced MRI of the myocardium. *Heart* 2019;**105**:1695–700.
35. Jiang Y, Zheng W. Cardiovascular toxicities upon manganese exposure. *CT* 2005;**5**:345–54.
36. Sutcliffe RP, Lewis D, Kane PA, Portmann BC, O'Grady JG, Karani JB *et al.* Manganese-enhanced MRI predicts the histological grade of hepatocellular carcinoma in potential surgical candidates. *Clin Radiol* 2011;**66**:237–43.
37. US Food and Drug Administration (FDA): teslascan (mangafodipir trisodium), 2002. https://www.accessdata.fda.gov/scripts/cder/daf/index.cfm?event=overview.process&ApplNo=020652 (June 2020, date last accessed).
38. European Medicines Agency: teslascan (mangafodipir): EPAR summary for the public, 2012. https://www.ema.europa.eu/en/medicines/human/EPAR/teslascan (June 2020, date last accessed).
39. Federle MP, Chezmar JL, Rubin DL, Weinreb JC, Freeny PC, Semelka RC *et al.* Safety and efficacy of mangafodipir trisodium (MnDPDP) injection for hepatic MRI in adults: results of the U.S. multicenter phase III clinical trials (safety). *J Magn Reson Imaging* 2000;**12**:186–97.
40. Martí-Bonmatí L, Fog AF, Beeck BO, de Kane P, Fagertun H. Safety and efficacy of mangafodipir trisodium in patients with liver lesions and cirrhosis. *Eur Radiol* 2003;**13**:1685–92.
41. Jynge P, Brurok H, Asplund A, Towart R, Refsum H, Karlsson JOG. Cardiovascular safety of MnDPDP and MnCl2. *Acta Radiol* 1997;**38**:740–9.